Science

Cite as: I. M. Hayes *et al.*, *Science*
10.1126/science.abb0272 (2021).

Multicomponent superconducting order parameter in UTe_2

I. M. Hayes[1]†, D. S. Wei[2,3]†, T. Metz[1], J. Zhang[4], Y. S. Eo[1], S. Ran[1,5], S. R. Saha[1,5], J. Collini[1], N. P. Butch[1,5], D. F. Agterberg[6], A. Kapitulnik[2,3,7,8]*, J. Paglione[1,5,9]*

[1]Department of Physics, Quantum Materials Center, University of Maryland, College Park, MD 20742, USA. [2]Geballe Laboratory for Advanced Materials, Stanford University, Stanford, CA 94305, USA. [3]Department of Applied Physics, Stanford University, Stanford, CA 94305, USA. [4]State Key Laboratory of Surface Physics, Department of Physics, Fudan University, Shanghai 200433, China. [5]NIST Center for Neutron Research, National Institute of Standards and Technology, Gaithersburg, MD 20899, USA. [6]Department of Physics, University of Wisconsin–Milwaukee, Milwaukee, WI 53201, USA. [7]Department of Physics, Stanford University, Stanford, CA 94305, USA. [8]Stanford Institute for Materials and Energy Sciences (SIMES), SLAC National Accelerator Laboratory, 2575 Sand Hill Road, Menlo Park, CA 94025, USA. [9]The Canadian Institute for Advanced Research, Toronto, Ontario, Canada. *Corresponding author. Email: paglione@umd.edu (J.P.); aharonk@stanford.edu (A.K.)

†These authors contributed equally to this work. *Corresponding author. Email: paglione@umd.edu (J.P.); aharonk@stanford.edu (A.K.)

An unconventional superconducting state was recently discovered in UTe_2, where spin-triplet superconductivity emerges from the paramagnetic normal state of a heavy fermion material. The coexistence of magnetic fluctuations and superconductivity, together with the crystal structure of this material, suggest that a unique set of symmetries, magnetic properties, and topology underlie the superconducting state. Here, we report observations of a non-zero polar Kerr effect and of two transitions in the specific heat upon entering the superconducting state, which together suggest that the superconductivity in UTe_2 is characterized by a two-component order parameter that breaks time reversal symmetry. These data place constraints on the symmetries of the order parameter and inform the discussion on the presence of topological superconductivity in UTe_2.

Unconventional superconductors can host topologically protected edge states provided that the right set of symmetries is broken at the superconducting transition temperature, T_c. The superconducting state of UTe_2 has attracted immense attention because several observations, including a temperature-independent NMR Knight shift (*1*), an anomalously large upper critical field (Hc_2) (*1*, *2*), re-entrant superconductivity at high fields (*3*), chiral behavior imaged by STM (*4*), and a point-node gap structure (*5*), all point to an odd-parity, spin-triplet pairing state. However, the key question of whether time reversal symmetry is broken remains open. A prior attempt to measure time reversal symmetry breaking (TRSB) in UTe_2 using muon spin relaxation was unsuccessful because of the presence of dynamic local magnetic fields (*6*). Furthermore, TRSB in UTe_2 seems unlikely as the irreducible point group (D_{2h}) representations of the orthorhombic crystal symmetry of UTe_2 are all one dimensional (*7*). For a superconducting order parameter to break time-reversal symmetry, it needs to have two components with a relative phase. Owing to the presence of strong spin-orbit coupling in UTe_2, which can be inferred from the strong anisotropy in its magnetic susceptibility (*1*), this means that the two components must belong to different irreducible representations of D_{2h}. This would necessarily result in multiple superconducting transitions, a rare phenomenon only exhibited by three other systems: UPt_3, Th-doped UBe_{13} and $PrOs_4Sb_{12}$ (*8*–*10*). In this study, we propose a multi-component order parameter that is experimentally supported by measurements of TRSB in UTe_2, as well as two distinct phase transitions in specific heat measurements. Together, these experiments allow us to strongly constrain the symmetry classification of the order parameters to two unique candidates.

To test for possible time reversal symmetry breaking (TRSB) in the superconducting state of UTe_2, we performed high resolution polar Kerr effects (PKE) measurements using a Zero-Area Sagnac Interferometer (*11*) (ZASI). In general, the generation of a Kerr effect arises from the unequal reflection (in both polarization and phase) of left and right circularly polarized light from a given material, resulting in reflected light relative to the incident light that is phase-shifted by a Kerr angle θ_K. The Kerr effect is not sensitive to Meissner effects, which normally prevent the measurement of global magnetic effects, and is therefore an optimal probe of TRSB in a superconducting system. At the same time, probing the system at frequencies (ω) much larger than the superconducting gap energy (Δ) will reduce a typical ferromagnetic-like signal of order ~1 rad, by a factor of $(\Delta/\hbar\omega)^2 \sim 10^{-7}$, where $\hbar$ is the reduced Planck constant, yielding a typical theoretically predicted signal of about 0.1-1 μrad (*12*–*18*). However, owing to the high degree of common-mode rejection of the ZASI for any reciprocal effects (e.g., linear birefringence, optical activity, etc.), we are able to detect these small signals.

The design and operation of our ZASI interferometer is detailed in references (*11*, *19*), and the basic operation is as follows: polar Kerr measurements are performed with 1550 nm wavelength light (20 uW incident power) that is polarized and then directed into a two-axes polarization maintaining optical fiber that threads down into a He-3 cryostat until it reaches our UTe_2 sample, which is mounted to a copper stage thermally anchored to the cold finger of the cryostat. There, a beam along each axis is reflected off the UTe_2 crystal face (incident on the a-b plane of the crystal) and launched back up the opposite axis of the fiber. The two reflected beams which have both traveled along identical paths (passing through the same optical plates, lenses, and fiber axes) compose the arms of the Sagnac interferometer. Any relative phase shift between the two beams must arise from encountering the sample, and are revealed upon interference with one another to produce a signal from which the Kerr angle rotation can be extracted. The UTe_2 single crystal used in this study and a basic schematic of the setup is shown in Fig. 1, A and B. Previously, this technique has been used to confirm TRSB in Sr_2RuO_4 (*20*) with a low-temperature saturation value of the Kerr effect of ~0.1 μrad. The heavy fermion uranium-based superconductors superconductors UPt_3 (*21*) and URu_2Si_2 (*22*), and the filled-skutterdite $PrOs_4Sb_{12}$ (*23*) gave a larger signal of ~0.4 to 0.7 μrad, which is expected owing to their strong spin-orbit interaction. Crucially, testing the apparatus with reciprocal reflecting media such as simple conventional superconductors, gold mirrors, and the spin-singlet d-wave heavy-fermion compound $CeCoIn_5$ (*24*), have yielded an expected null result.

To begin, we report the results of polar Kerr measurements performed at low temperatures on a single crystal of UTe_2. The sample was first cooled below T_c of UTe_2 (~1.6K) in ambient magnetic field (H_{ext} <0.3Oe), and the Kerr angle was subsequently measured as the sample was warmed above T_c. We find a small (~400 nrad at 300mK), field-trainable Kerr effect that onsets near T_c ~ 1.6K, which is consistent with a TRSB superconducting order parameter; Fig. 1C shows two runs performed identically in this manner. Whereas Run 1 shows a signal emerging around T_c, and saturating at ~500 nrad, Run 2 shows no discernible signal. This indicates that without an applied field, domains are formed in the sample that can orient in opposite directions, and give a finite signal or no signal at all, with an average signal of zero and a standard deviation dependent on the domain to beam size (10 um) (*11*). Similar results were found for a second UTe_2 crystal, from a separate growth batch (fig. S1A). The detection of a finite positive Kerr signal indicates that a spontaneously large domain forms upon cooling the sample, due to TRSB in UTe_2.

To orient all of the domains in one direction, the sample was cooled through T_c in a small applied field of +25 Gauss. Experimentally, the magnitude of this training field has been found to be on the order of the lower superconducting critical field, H_{c1} (*21*). Once the sample reaches base temperature (~300mK), the external field is removed, and the Kerr angle is measured as the sample is warmed slowly up past T_c. Figure 2 shows a positive finite Kerr value develop around T_c in this zero-field measurement. The sign of θ_K is reversed with a negative training field (-25 Gauss), indicating that the broken time-reversal symmetry shares the same symmetry as a magnetic moment. This is because trainability with field implies a linear coupling between the field and broken time-reversal symmetric order parameter.

The magnitude of the trained signal should indicate the maximum signal size when all of the domains are aligned in the same direction. Depending on the size of the domains as the sample is cooled through T_c, the signal can be very small, or close to the full signal that can be achieved with field-training field (see e.g., data on UPt_3 in ref. 21). This may depend on the size of the sample, its purity and thus ability to pin domains, and the size of the probing beam. Additionally, small differences between signals in different runs may arise extrinsically owing to a change in background noise (from optical and electronic components and equipment) between runs. The measured Kerr signal was found to be independent of the magnitude of a small, applied training field (fig. S1B), indicating that the signal does not arise from magnetic vortices in the sample.

As discussed above, a TRSB order parameter in UTe_2 can only be built out of two components belonging to two different irreducible representations (*25*). This makes UTe_2 different from $LaNiGa_2$, which also hosts TRSB superconductivity that develops out of a paramagnetic state (*26*). In that material, which also has a D_{2h} point group, a multidimensional representation can be obtained by including the spin degree of freedom, an option that is precluded in UTe_2 owing to spin-orbit coupling. It is exceptionally rare for a system to support superconducting transitions in two symmetry channels, which might caution against our interpretation. However, we find direct evidence for the existence of two superconducting order parameters in the specific heat of UTe_2. Normally, superconducting states are identified by resistivity or magnetization measurements, but neighboring superconducting states would both show zero resistance and diamagnetism. For this reason, specific heat measurements have played a central role in identifying all previous examples of superconductors with multicomponent order parameters (*8*–*10*).

The specific heat at zero field was first measured using the small-pulse method with $\Delta T = 0.5 - 1\%$ (*27*). Four single crystals were measured from two growth batches (*28*). Figure 3 shows C_p/T near the superconducting transition for these four samples. In each case there is a shoulder-like feature at a temperature about 75 - 100mK above the peak in C_p/T. This feature is quite sharp and divides the jump in the specific heat into two local maxima in the derivative, $d(C_p/T)/dT$, representing two thermodynamic anomalies. The existence of two transitions seems to be stable to whatever perturbations are responsible for the notable difference in T_c between sample S4 and samples S1, S2, and S3. An additional three samples from a third growth batch also show two transitions (fig. S4). The consistent splitting of T_c across seven samples despite differences in growth conditions and absolute value of T_c provides firm support for our inference that this splitting is intrinsic to UTe_2, reflecting the presence of a multicomponent order parameter, and is not an artifact of inclusions or intergrowths in these crystals. Furthermore, the inclusion scenario would not help explain the observed Kerr signal, because the order parameter has to have two components locally for a Kerr effect to exist. This is an essential point; prior observations of split superconducting transitions were only accepted slowly by the community because of the possibility that the two observed transitions were the result of inhomogeneity in the crystals. However, the fact that both the specific heat data and the polar Kerr data point to a two-component order parameter in UTe_2 makes the conclusion compelling in the present case. This is especially true given that these two measurements probe the material on different scales: a 10 μm spot on the surface in the case of the Kerr effect, and the bulk of the crystal in the case of specific heat. Finally, recent work has shown that there are two well-separated transitions under pressure (*29*, *30*), which supports the idea that there are two nearly degenerate symmetry breaking possibilities for a superconducting state in UTe_2. Both studies show that the splitting diminishes rapidly with decreasing pressure, with one study confirming the existence of splitting at ambient pressure (*30*), suggesting that the small splitting evident in our heat capacity experiments may be sensitive to sample quality and difficult to discern in other published work (*2*, *31*).

Beyond demonstrating that the order parameter in UTe_2 is two-component and TRSB, our data provide strong constraints on the particular irreducible representations to which the two components of the order parameter belong. Our observation that the TRSB in UTe_2 can be trained by a magnetic field along the crystallographic *c*-axis requires the presence of a term $\sim iH_c(\psi_1\psi_2^* - \psi_1^*\psi_2)$ in the free energy, where H_c is the *c*-axis component of the magnetic field and ψ_1, ψ_2 are the two components of the superconducting order parameter. Symmetry requires that this term exists for only four possibilities (*28*):

1 - $\psi_1 \in B_{3u}$ and - $\psi_2 \in B_{2u}$

2 - $\psi_1 \in B_{1u}$ and - $\psi_2 \in A_u$

3 - $\psi_1 \in B_{3g}$ and - $\psi_2 \in B_{2g}$

4 - $\psi_1 \in B_{1g}$ and - $\psi_2 \in A_{1g}$

using the notation for irreducible representations adopted in Ref. (*5*). However, because UTe_2 is known to be a spin-triplet superconductor, we can narrow the possibilities to the first two: B_{3u} and B_{2u}, or B_{1u} and A_u.

This picture can be checked by studying the two superconducting transitions as a function of magnetic field. The symmetry considerations that suggest that TRSB can be trained with a field applied along the *c*-axis imply that the lower temperature transition should broaden and vanish with increasing field applied along that direction. This follows from the fact that the term $\sim iH_c(\psi_1\psi_2^* - \psi_1^*\psi_2)$ leads to a linear coupling between the two order parameters when a *c*-axis field is present. Symmetry considerations preclude the existence of terms like these for fields along the *a*- and *b*-axes. Therefore, we expect the two transitions to remain distinct when a magnetic field is applied along those axes, but not when a field is applied along the *c*-axis.

The field dependence of the split T_c transition was measured on samples S1 and S2 by a large-pulse method (*28*) using oriented fields up to 5T in a vector magnet (Fig. 4). The crystal orientation was determined by measuring the field angle dependent T_c for a field of 2T. For fields oriented along the *a*- and *b*-axes, there are two discernable features at all fields. For field along the c-axis, the two transitions broaden in field so that the splitting is no longer discernable above ~2T, consistent with what we expected based on the trainability of the TRSB with a *c*-axis field. The fact that both the trainability of the Kerr signal and the magnetic field dependence of the specific heat point to the same symmetry classification of the order parameters confirms that the two phenomena are connected and intrinsic to UTe_2.

We thus arrive at a consistent picture of a superconducting state characterized by two order parameters that belong either to B_{3u} and B_{2u}, or B_{1u} and A_u, and that have a relative phase of $\pi/2$, leading to a TRSB state. Next, we turn to the question of the appearance of nodes. Thermal conductivity and penetration depth measurements suggest point node excitations (*5*). These have been interpreted as originating from the symmetry required points nodes of a time-reversal invariant odd-parity state (*5*). Naively, TRSB gaps these point nodes, leading to a fully gapped state which appears inconsistent with these experiments (*5*). However, topological arguments allow for the possibility of Weyl point nodes (*32*–*34*), which we now consider in more detail. Weyl nodes are topologically protected by an integer Chern number, *Z,* and have associated surface Fermi arc states (*32*–*34*). For an odd-parity superconducting state in a Kramer's doubly degenerate pseudo-spin band, the single-particle gaps in the quasiparticle spectrum for the two pseudo-spin-species are in general different and are given by (*25*)

$$E_{+/-} = \sqrt{\left(\epsilon(k) - \mu\right)^2 + \left|\boldsymbol{d}(k)\right|^2 \pm \left|\boldsymbol{q}(k)\right|^2}$$

Here the gap function is $\Delta(k) = \left[\boldsymbol{d}(k)\cdot\boldsymbol{\sigma}\right]\left(i\boldsymbol{\sigma}_y\right)$ (with Pauli matrices acting in pseudo-spin space), and $\boldsymbol{q}(k) = \boldsymbol{d}(k)\times\boldsymbol{d}^*(k)$ denotes the non-unitary part that naturally arises when time reversal symmetry is broken. In the two possibilities discussed above, the gap function is given by $\boldsymbol{d} = \boldsymbol{d}_1 + i\boldsymbol{d}_2$, where $\boldsymbol{d}_1$ and $\boldsymbol{d}_2$ are both real. This gap function then gives rise to the single particle gaps

$$|\Delta_\pm|^2 = |\boldsymbol{d}(k)|^2 \pm |\boldsymbol{q}(k)|^2 = |\boldsymbol{d}_1|^2 + |\boldsymbol{d}_2|^2 \pm 2|\boldsymbol{d}_1 \times \boldsymbol{d}_2|$$
$$= |\boldsymbol{d}_1|^2 + |\boldsymbol{d}_2|^2 \pm 2\sin\theta |\boldsymbol{d}_1| |\boldsymbol{d}_2|$$

where θ is the angle between $\boldsymbol{d}_1$ and $\boldsymbol{d}_2$. Nodes can only appear in Δ_- and for this to occur two conditions must be met: i) $\boldsymbol{d}_1 \cdot \boldsymbol{d}_2 = 0$ ($\sin\theta = 1$) and ii) $|\boldsymbol{d}_1| = |\boldsymbol{d}_2|$. In general, these two conditions will be satisfied on a line in momentum space. If this line intersects the Fermi surface, there will be a Weyl point. If it does not, the superconductor will be fully gapped. Consequently, for the two gap structures discussed above, Weyl nodes can occur at arbitrary momenta on the Fermi surface.

Although the above argument reveals that Weyl points can generically occur, it does not guarantee that they exist in UTe_2. Surprisingly, it can be shown that Weyl points are expected for the $B_{2u} + iB_{3u}$ state. Given the current lack of detailed understanding of the electronic structure that gives rise to superconductivity, it is not possible to precisely identify the momentum dependence of the gap structure. However, symmetry places constraints on this. The symmetry dictated form of the of the corresponding gap functions are $\boldsymbol{d}_{B2u} = f_{z,2}(\boldsymbol{k})\hat{x} + f_{u,2}(\boldsymbol{k})\hat{y} + f_{x,2}(\boldsymbol{k})\hat{z}$ and $\boldsymbol{d}_{B3u} = f_{u,3}(\boldsymbol{k})\hat{x} + f_{z,3}(\boldsymbol{k})\hat{y} + f_{y,3}(\boldsymbol{k})\hat{z}$, where the unknown functions $f_{x,i}, f_{y,i}, f_{z,i}, f_{u,i}$ share the same symmetry properties as $k_x, k_y, k_z, k_x k_y k_z$. To find Weyl points for such a gap it is helpful to use insight for the Weyl semi-metal $MoTe_2$ where it was found that Weyl points appear in mirror planes (*35*). In particular, consider $k_x = 0$, then $f_{x,i} = f_{u,i} = 0$ by symmetry. This immediately implies $\boldsymbol{d}_{B2u} \cdot \boldsymbol{d}_{B3u} = 0$ in this mirror plane. Furthermore, the nodal condition $|\boldsymbol{d}_{B2u}| = |\boldsymbol{d}_{B3u}|$ implies that $\tilde{g}_z \equiv f_{z,2}{}^2 - f_{z,3}{}^2 = f_{y,3}{}^2$. It is also possible to carry out a similar analysis for the mirror plane $k_y = 0$, for which $\boldsymbol{d}_{B2u} \cdot \boldsymbol{d}_{B3u} = 0$ is also satisfied. In this case, $|\boldsymbol{d}_{B2u}| = |\boldsymbol{d}_{B3u}|$ implies $-\tilde{g}_z = f_{x,2}{}^2$. The relative minus sign in the two expressions $\tilde{g}_z = f_{y,3}{}^2$ ($k_x = 0$) and $-\tilde{g}_z = f_{x,2}{}^2$ ($k_y = 0$) ensures Weyl point will exist, provided that the cross section of the Fermi surface in both the k_x and $k_y = 0$ planes has a circular topology (to see, this note that $\tilde{g}_z = 0$ for $k_z = 0$, $f_{x,i} = 0$, $k_x = 0$ and $f_{y,i} = 0$ for $k_y = 0$ so that one of these two expressions must be satisfied somewhere on a closed Fermi surface encircling the origin in the $k_z - k_x$ or $k_z - k_y$ planes). Recent angle-resolved photoemission experiments suggest that such a Fermi surface exists (*36*), revealing a likely *f*-electron derived Fermi surface surrounding the *Z* point in the Brillouin zone. Consequently, this state will give rise to at least four Weyl points in either the $k_x = 0$ or the $k_y = 0$ planes. A similar analysis for the $A_u + iB_{1u}$ state (*28*) shows that, in this case, Weyl nodes are not guaranteed but are likely.

The above considerations, together with prior evidence for point nodes in UTe_2 from thermal conductivity and penetration depth measurements (*5*), support the conclusion that UTe_2 is a Weyl superconductor. The Weyl points in the superconducting gap would give rise to surface Fermi arc states, providing a natural explanation for the observation of chiral surface states (*4*). These findings suggest the possibility of using UTe_2 for topological quantum computing, as well as for the exploration of superconducting analogs to phenomena in Weyl semimetals, including Fermi arcs and unusual Hall effects (*37*).

REFERENCES AND NOTES

1. S. Ran, C. Eckberg, Q. P. Ding, Y. Furukawa, T. Metz, S. R. Saha, I. L. Liu, M. Zic, H. Kim, J. Paglione, N. P. Butch, Nearly ferromagnetic spin-triplet superconductivity. *Science* **365**, 684–687 (2019). doi:10.1126/science.aav8645 Medline
2. D. Aoki, A. Nakamura, F. Honda, D. Li, Y. Homma, Y. Shimizu, Y. J. Sato, G. Knebel, J.-P. Brison, A. Pourret, D. Braithwaite, G. Lapertot, Q. Niu, M. Vališka, H. Harima, J. Flouquet, Unconventional Superconductivity in Heavy Fermion UTe_2. *J. Phys. Soc. Jpn.* **88**, 043702 (2019). doi:10.7566/JPSJ.88.043702
3. S. Ran, I.-L. Liu, Y. S. Eo, D. J. Campbell, P. M. Neves, W. T. Fuhrman, S. R. Saha, C. Eckberg, H. Kim, D. Graf, F. Balakirev, J. Singleton, J. Paglione, N. P. Butch, Extreme magnetic field-boosted superconductivity. *Nat. Phys.* **15**, 1250–1254 (2019). doi:10.1038/s41567-019-0670-x Medline
4. L. Jiao, S. Howard, S. Ran, Z. Wang, J. O. Rodriguez, M. Sigrist, Z. Wang, N. P. Butch, V. Madhavan, Chiral superconductivity in heavy-fermion metal UTe_2. *Nature* **579**, 523–527 (2020). doi:10.1038/s41586-020-2122-2 Medline
5. T. Metz, S. Bae, S. Ran, I.-L. Liu, Y. S. Eo, W. T. Fuhrman, D. F. Agterberg, S. M. Anlage, N. P. Butch, J. Paglione, Point-node gap structure of the spin-triplet superconductor UTe_2. *Phys. Rev. B* **100**, 220504 (2019). doi:10.1103/PhysRevB.100.220504 Medline
6. S. Sundar, S. Gheidi, K. Akintola, A. M. Côté, S. R. Dunsiger, S. Ran, N. P. Butch, S. R. Saha, J. Paglione, J. E. Sonier, Coexistence of ferromagnetic fluctuations and superconductivity in the actinide superconductor UTe_2. *Phys. Rev. B* **100**, 140502 (2019). doi:10.1103/PhysRevB.100.140502 Medline
7. V. Hutanu, H. Deng, S. Ran, W. T. Fuhrman, H. Thoma, N. P. Butch, Low-temperature crystal structure of the unconventional spin-triplet superconductor UTe_2 from single-crystal neutron diffraction. *Acta Crystallogr. B* **76**, 137 (2020). doi:10.1107/S2052520619016950 Medline
8. R. Joynt, L. Taillefer, The superconducting phases of UPt_3. *Rev. Mod. Phys.* **74**, 235–294 (2002). doi:10.1103/RevModPhys.74.235
9. H. R. Ott, H. Rudigier, Z. Fisk, J. L. Smith, Phase transition in the superconducting state of $U_{1-x}Th_xBe_{13}$ (x=0-0.06). *Phys. Rev. B Condens. Matter* **31**, 1651–1653 (1985). doi:10.1103/PhysRevB.31.1651 Medline
10. M. B. Maple, P.-C. Ho, V. S. Zapf, N. A. Frederick, E. D. Bauer, W. M. Yuhasz, F. M. Woodward, J. W. Lynn, Heavy Fermion Superconductivity in the Filled Skutterudite Compound $PrOs_4Sb_{12}$. *J. Phys. Soc. Jpn.* **71**, 23–28 (2002). doi:10.1143/JPSJS.71S.23
11. J. Xia, P. T. Beyersdorf, M. M. Fejer, A. Kapitulnik, Modified Sagnac interferometer for high-sensitivity magneto-optic measurements at cryogenic temperatures. *Appl. Phys. Lett.* **89**, 062508 (2006). doi:10.1063/1.2336620
12. J. Goryo, Impurity-induced polar Kerr effect in a chiral p-wave superconductor.

Phys. Rev. B Condens. Matter Mater. Phys. **78**, 060501 (2008). doi:10.1103/PhysRevB.78.060501

13. R. M. Lutchyn, P. Nagornykh, V. M. Yakovenko, Frequency and temperature dependence of the anomalous ac Hall conductivity in a chiral p_x+i p_y superconductor with impurities. *Phys. Rev. B Condens. Matter Mater. Phys.* **80**, 104508 (2009). doi:10.1103/PhysRevB.80.104508
14. E. Taylor, C. Kallin, Intrinsic Hall effect in a multiband chiral superconductor in the absence of an external magnetic field. *Phys. Rev. Lett.* **108**, 157001 (2012). doi:10.1103/PhysRevLett.108.157001 Medline
15. P. M. R. Brydon, D. S. L. Abergel, D. F. Agterberg, V. M. Yakovenko, Loop Currents and Anomalous Hall Effect from Time-Reversal Symmetry-Breaking Superconductivity on the Honeycomb Lattice. *Phys. Rev. X* **9**, 031025 (2019). doi:10.1103/PhysRevX.9.031025
16. E. J. König, A. Levchenko, Kerr Effect from Diffractive Skew Scattering in Chiral p_x±ip_y Superconductors. *Phys. Rev. Lett.* **118**, 027001 (2017). doi:10.1103/PhysRevLett.118.027001 Medline
17. K. I. Wysokiński, J. F. Annett, B. L. Györffy, Intrinsic optical Dichroism in the 2D model of Chiral superconducting state. *J. Supercond. Nov. Magn.* **26**, 1909–1913 (2013). doi:10.1007/s10948-012-2046-7
18. M. Gradhand, K. I. Wysokinski, J. F. Annett, B. L. Györffy, Kerr rotation in the unconventional superconductor Sr_2RuO_4. *Phys. Rev. B Condens. Matter Mater. Phys.* **88**, 094504 (2013). doi:10.1103/PhysRevB.88.094504
19. A. Kapitulnik, J. Xia, E. Schemm, A. Palevski, Polar Kerr effect as probe for time-reversal symmetry breaking in unconventional superconductors. *New J. Phys.* **11**, 055060 (2009). doi:10.1088/1367-2630/11/5/055060
20. J. Xia, Y. Maeno, P. T. Beyersdorf, M. M. Fejer, A. Kapitulnik, High resolution polar Kerr effect measurements of Sr_2RuO_4: Evidence for broken time-reversal symmetry in the superconducting state. *Phys. Rev. Lett.* **97**, 167002 (2006). doi:10.1103/PhysRevLett.97.167002 Medline
21. E. R. Schemm, W. J. Gannon, C. M. Wishne, W. P. Halperin, A. Kapitulnik, Observation of broken time-reversal symmetry in the heavy-fermion superconductor UPt_3. *Science* **345**, 190–193 (2014). doi:10.1126/science.1248552 Medline
22. E. R. Schemm, R. E. Baumbach, P. H. Tobash, F. Ronning, E. D. Bauer, A. Kapitulnik, Evidence for broken time-reversal symmetry in the superconducting phase of URu_2Si_2. *Phys. Rev. B Condens. Matter Mater. Phys.* **91**, 140506 (2015). doi:10.1103/PhysRevB.91.140506
23. E. M. Levenson-Falk, E. R. Schemm, Y. Aoki, M. B. Maple, A. Kapitulnik, Polar Kerr Effect from Time-Reversal Symmetry Breaking in the Heavy-Fermion Superconductor $PrOs_4Sb_{12}$. *Phys. Rev. Lett.* **120**, 187004 (2018). doi:10.1103/PhysRevLett.120.187004 Medline
24. E. R. Schemm, E. M. Levenson-Falk, A. Kapitulnik, Polar Kerr effect studies of time reversal symmetry breaking states in heavy fermion superconductors. *Phys. C Supercond. Its Appl.* **535**, 13–19 (2017). doi:10.1016/j.physc.2016.11.012
25. M. Sigrist, K. Ueda, Phenomenological theory of unconventional superconductivity. *Rev. Mod. Phys.* **63**, 239–311 (1991). doi:10.1103/RevModPhys.63.239
26. A. D. Hillier, J. Quintanilla, B. Mazidian, J. F. Annett, R. Cywinski, Nonunitary triplet pairing in the centrosymmetric superconductor $LaNiGa_2$. *Phys. Rev. Lett.* **109**, 097001 (2012). doi:10.1103/PhysRevLett.109.097001 Medline
27. R. Bachmann, F. J. DiSalvo Jr., T. H. Geballe, R. L. Greene, R. E. Howard, C. N. King, H. C. Kirsch, K. N. Lee, R. E. Schwall, H. U. Thomas, R. B. Zubeck, Heat capacity measurements on small samples at low temperatures. *Rev. Sci. Instrum.* **43**, 205–214 (1972). doi:10.1063/1.1685596
28. Supplemental Materials, available online.
29. D. Braithwaite, M. Vališka, G. Knebel, G. Lapertot, J.-P. Brison, A. Pourret, M. E. Zhitomirsky, J. Flouquet, F. Honda, D. Aoki, Multiple superconducting phases in a nearly ferromagnetic system. *Commun. Phys.* **2**, 147 (2019). doi:10.1038/s42005-019-0248-z
30. S. M. Thomas, F. B. Santos, M. H. Christensen, T. Asaba, F. Ronning, J. D. Thompson, E. D. Bauer, R. M. Fernandes, G. Fabbris, P. F. S. Rosa, Evidence for a pressure-induced antiferromagnetic quantum critical point in intermediate-valence UTe_2. *Sci. Adv.* **6**, eabc8709 (2020). doi:10.1126/sciadv.abc8709 Medline
31. L. P. Cairns, C. R. Stevens, C. D. O'Neill, A. Huxley, Composition dependence of the superconducting properties of UTe_2. *J. Phys. Condens. Matter* **32**, 415602 (2020). doi:10.1088/1361-648X/ab9c5d Medline
32. V. Kozii, J. W. F. Venderbos, L. Fu, Three-dimensional Majorana fermions in chiral superconductors. *Sci. Adv.* **2**, e1601835 (2016). doi:10.1126/sciadv.1601835 Medline
33. K. Shiozaki, M. Sato, Topology of Crystalline Insulators and Superconductors. *Phys. Rev. B Condens. Matter Mater. Phys.* **90**, 165114 (2014). doi:10.1103/PhysRevB.90.165114
34. T. Bzdušek, M. Sigrist, Robust Doubly Charged Nodal Lines and Nodal Surfaces in Centrosymmetric Systems. *Phys. Rev. B* **96**, 155105 (2017). doi:10.1103/PhysRevB.96.155105
35. Z. Wang, D. Gresch, A. A. Soluyanov, W. Xie, S. Kushwaha, X. Dai, M. Troyer, R. J. Cava, B. A. Bernevig, MoTe2: A Type-II Weyl Topological Metal. *Phys. Rev. Lett.* **117**, 1–5 (2016).
36. L. Miao, S. Liu, Y. Xu, E. C. Kotta, C.-J. Kang, S. Ran, J. Paglione, G. Kotliar, N. P. Butch, J. D. Denlinger, L. A. Wray, Low Energy Band Structure and Symmetries of UTe_2 from Angle-Resolved Photoemission Spectroscopy. *Phys. Rev. Lett.* **124**, 076401 (2020). doi:10.1103/PhysRevLett.124.076401 Medline
37. B. Yan, C. Felser, Topological Materials: Weyl Semimetals. *Annu. Rev. Condens. Matter Phys.* **8**, 337–354 (2017). doi:10.1146/annurev-conmatphys-031016-025458
38. I. M. Hayes *et al*., Replication Data for, "Multi-component Superconducting Order Parameter in UTe_2," Zenodo (2021); https://doi.org/10.5281/zenodo.4924576.
39. M. B. Walker, K. V. Samokhin, Model for superconductivity in ferromagnetic $ZrZn_2$. *Phys. Rev. Lett.* **88**, 207001 (2002). doi:10.1103/PhysRevLett.88.207001 Medline
40. A. Amin, D. F. Agterberg, Generalized spin fluctuation feedback in heavy fermion superconductors. *Phys Rev. Research* **2**, 013381 (2020). doi:10.1103/PhysRevResearch.2.013381
41. A. H. Nevidomskyy, Stability of a nonunitary triplet pairing on the border of magnetism in UTe2. arXiv:2001.02699 [cond-mat.supr-con] (2020).
42. V. G. Yarzhemsky, E. A. Teplyakov, Time-reversal symmetry and the structure of superconducting order parameter of nearly ferromagnetic spin-triplet superconductor UTe_2. arXiv:2001.02963. [cond-mat.supr-con] (2020).

ACKNOWLEDGMENTS

We thank E. Schemm, S. Tomarken, Philip Brydon, Tatsuya Shishidou, and Michael Weinert for useful discussions. **Funding:** Work at Stanford University was supported by the Department of Energy, Office of Basic Energy Sciences, under contract no. DE-AC02-76SF00515 and the Gordon and Betty Moore Foundation through Emergent Phenomena in Quantum Systems (EPiQS) Initiative Grant No. GBMF4529. Research at the University of Maryland was supported by the Air Force Office of Scientific Research Award No. FA9550-14-1-0332 (support of T.M.), the Department of Energy Award No. DE-SC-0019154 (specific heat experiments), the National Science Foundation Division of Materials Research Award DMR-1905891 (support of J.C.), the Gordon and Betty Moore Foundation's EPiQS Initiative through Grant No. GBMF9071 (materials synthesis), NIST, and the Maryland Quantum Materials Center. S.R.S acknowledges support from the National Institute of Standards and Technology Cooperative Agreement 70NANB17H301. D.S.W. acknowledges support from the Karel Urbanek Fellowship in Applied Physics at Stanford University. **Author contributions:** D.S.W., I.M.H., A.K and J.P. conceived and designed the experiments. S.R., S. R. S. and N.B. synthesized the UTe_2. S.R., S.R.S., and J.C. helped characterize the samples. D.S.W., J.Z. performed the polar Kerr effect measurements. I.M.H., T.M. and Y.S.E. performed the specific heat measurements. D.F.A. provided the theoretical analysis. I.M.H., D.S.W., T.M., S.R., N.B., D.F.A., J.P., and A.K. analyzed the data and wrote the paper. **Competing interests:** Authors declare no competing interests. **Data and materials availability:** The data presented in this manuscript are available at Zenodo (*38*).

SUPPLEMENTARY MATERIALS

science.sciencemag.org/cgi/content/full/science.abb0272/DC1
Materials and Methods
Supplementary Text
Figs. S1 to S4
Table S1

References (*39*–*42*)

5 February 2020; resubmitted 30 June 2020
Accepted 30 June 2021
Published online 15 July 2021

10.1126/science.abb0272

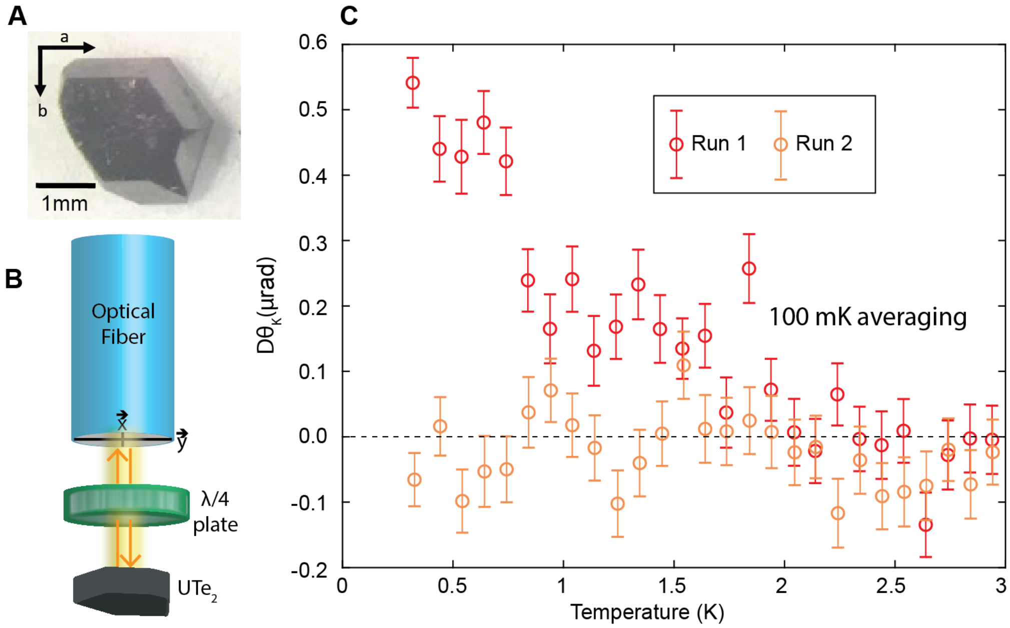

Fig. 1. Polar Kerr angle evolution across the superconducting transition temperature in UTe_2. (**A**) Optical image of the UTe_2 single crystal used in this work. (**B**) Schematic of the Sagnac interferometer used to measure the polar Kerr angle. The two orthogonal axes of the fiber compose the arms of the interferometer. Light from one axis is converted to circularly polarized light at the quarter-wave plate, reflected off the sample, and then converted back to linearly polarized light at the quarter-wave plate, and then transmitted into the axis orthogonal to the one from which is originated (focusing lenses are omitted for clarity). The light is reflected off of the a-b plane. (**C**) Kerr angle plotted as a function of increasing temperature, after the UTe_2 single crystal was cooled through the superconducting transition temperature (1.6K) with zero applied magnetic field. Error bars represent statistical error of hundreds of data points averaged together over 100 mK range bins (*28*). Two separate runs are shown. Run 1 shows no change in Kerr angle as the sample is cooled through T_c. Run 2 shows an increase in the Kerr angle around T_c, saturating at ~500 nrad.

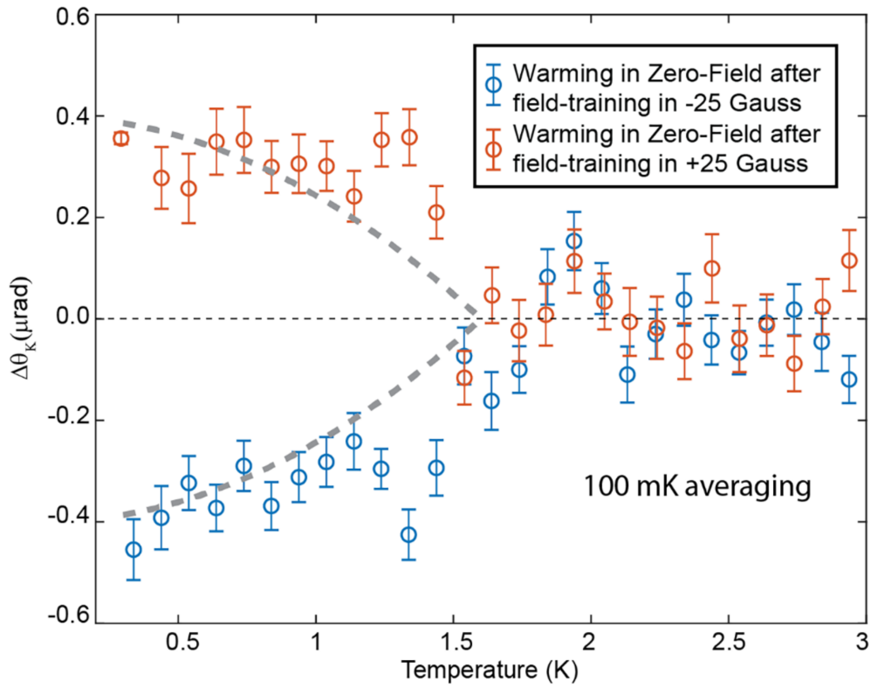

Fig. 2. Magnetic field training of the Kerr effect. Kerr angle for two different runs where the sample is warmed up past T_c after being cooled in an applied field. For a positive (negative) applied field of +25 Gauss (-25 Gauss) a positive (negative) Kerr signal emerges at T_c and saturates around ~400 nrad. Dashed lines are guides to the eye to indicate where the onset of the Kerr signal begins. The actual temperature dependence of the Kerr signal is expected to be more complicated thanks to coupling of the superconducting order parameter to the magnetic fluctuations.

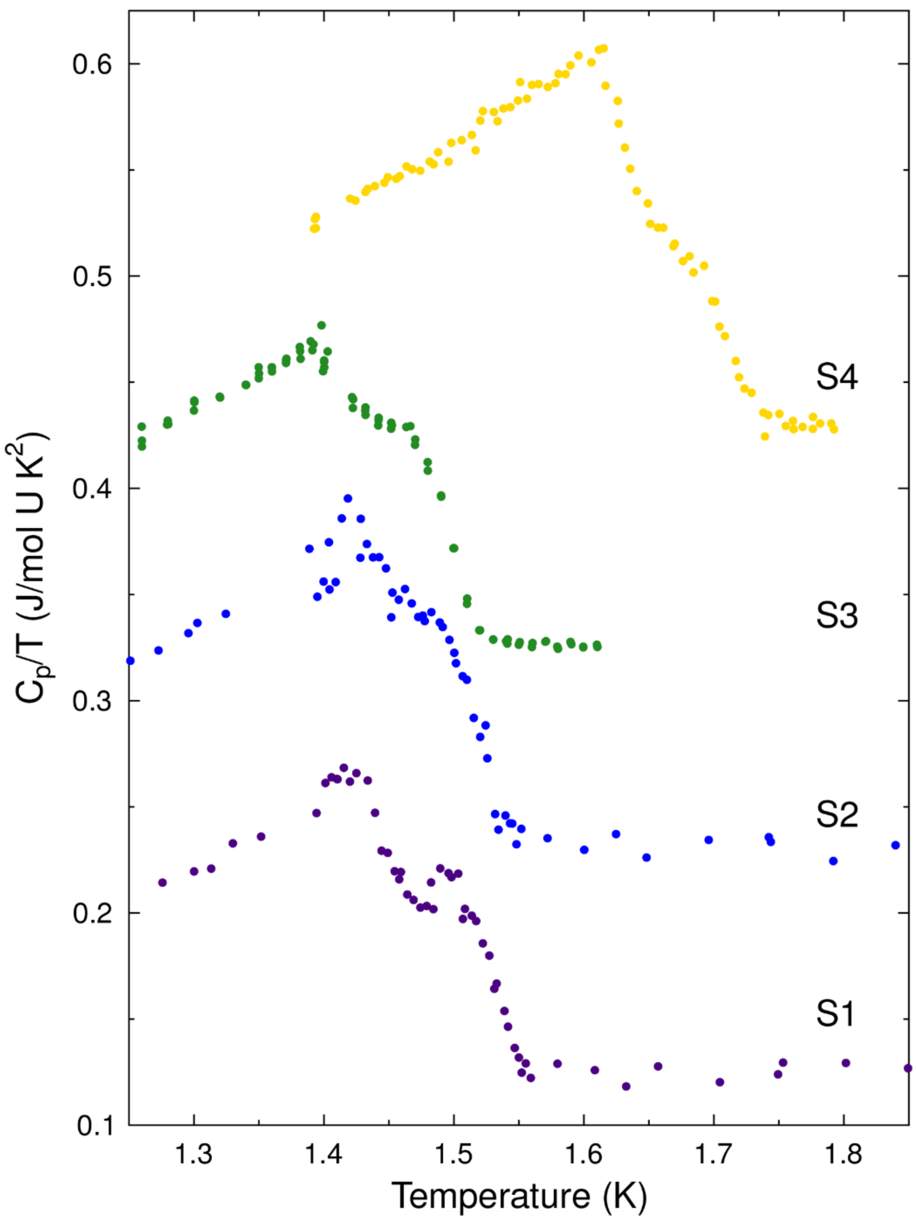

Fig. 3. Superconducting transitions of UTe_2 in specific heat. The specific heat over temperature per mole uranium is plotted versus temperature for four samples of UTe_2. The y-axis is accurate for sample S1 whereas the curves for the other three samples have been offset in increments of 100mJ/molK^2. Each sample shows two anomalies, separated by ~80mK, indicating the presence of two superconducting transitions. Samples S1-3 come from one growth batch whereas S4 comes from another (see fig. S4 (*28*) for further details and data on three additional samples).

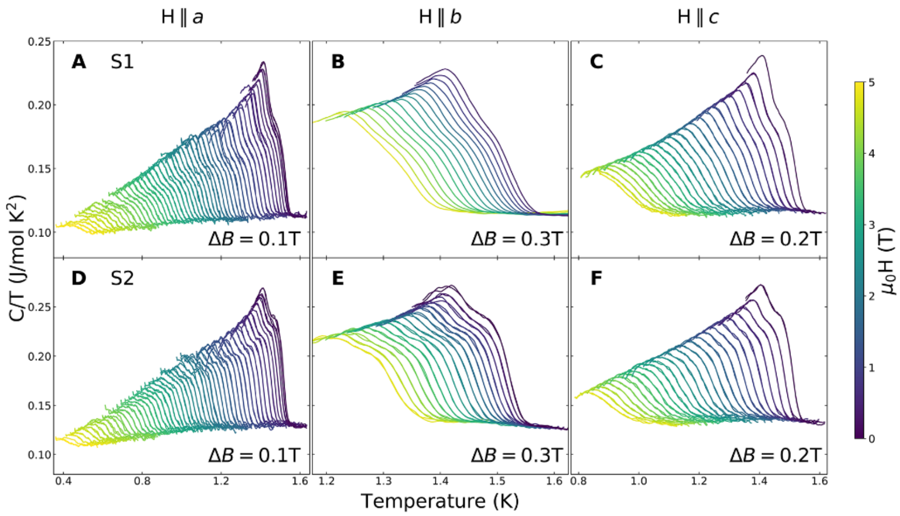

Fig. 4. Magnetic field evolution of the split superconducting transition of UTe_2. For samples S1 and S2, specific heat was measured by a long pulse method (see text for details) at every 100mT or 300mT along each of the crystallographic axes. Each panel corresponds to one field orientation for one of the samples and shows *Cp/T*(*T*) curves gathered at each magnetic field. The curves have not been offset. When the field is oriented along the crystallographic *c*-axis the two transitions are indistinguishable above ~2T, consistent with the linear field coupling to the product of the order parameters implied by Kerr data. However, for the other field orientations, two features are visible up to much higher magnetic fields.